

Minimal model for higher-order topological insulators and phosphorene

Motohiko Ezawa

Department of Applied Physics, University of Tokyo, Hongo 7-3-1, 113-8656, Japan

A higher order topological insulator is an extended notion of the conventional topological insulator, which belongs to a special class of topological insulators where the conventional bulk-boundary correspondence is not applicable. The bulk topological index may be described by the Wannier center located at a high symmetry point of the crystal. In this paper we propose minimal models for the second-order topological insulator in two dimensions and the third-order topological insulator in three dimensions. They are anisotropic two-band models with two different hopping parameters. The two-dimensional model is known to capture the essential physics of phosphorene near the Fermi level. It has so far been recognized as a trivial insulator due to the absence of topological edge states in nanoribbons. However, we demonstrate the emergence of topological boundary states in zero dimension, i.e., in nanodisks. In particular, the diamond structure exhibits such topological states at two corners, each of which carries a $1/2$ fractional charge. We predict that these corner states will be observed in the diamond structure of phosphorene.

A topological insulator (TI) is characterized by the bulk topological index together with the emergence of topological boundary states^{1,2}. The gap must close along the boundary since the topological index cannot change its value continuously across the boundary, which is known as the bulk-boundary correspondence. The typical bulk topological index is the Chern number, which is the genuine one. Another typical one is the Z_2 index, which is protected by the time-reversal symmetry. However, recently, the concept of the TI has been generalized to include the higher-order TI (HOTI)³⁻¹². Let us consider a j -dimensional (j D) bulk system. For instance, a second-order TI is an insulator which has $(j-2)$ D topological boundary states but no $(j-1)$ D topological boundary states. Similarly, a third-order TI is an insulator which has $(j-3)$ D topological boundary states but no $(j-1)$ D and $(j-2)$ D topological boundary states. Namely, the boundary of the third-order TI is the second-order TI. In spite of these properties, the HOTI is also characterized by the bulk topological index^{4,8,9,12}. It belongs to a special class of TIs to which the conventional bulk-boundary correspondence is not applicable. Accordingly, there must be HOTIs which have so far been regarded as trivial insulators.

Recent studies have revealed a crucial role that the Wannier center (WC) plays in a certain type of HOTIs^{4,8,9,12}. The WC is the expectation value of the position in the unit cell of a crystal and given by the integral of the Berry connection over the Brillouin zone. The WC is fixed at the high symmetry point. Since it is proved that its value is quantized in insulators, it can be used as a new type of the topological number^{4,8,9,12}. We consider the atomic insulator limit, where there are no interactions among any lattice sites. The WC is on the lattice site, and the system is a trivial insulator. In general, it is trivial when the WC is on the lattice site, and topological otherwise¹³⁻¹⁶.

Here we propose the minimal models of Wannier-type HOTIs in two and three dimensions. We first analyze a 2D crystal (anisotropic honeycomb lattice) possessing the chiral symmetry as the minimal model. In this model we show that the WC is identical to the winding number. We calculate the energy spectra for the bulk, the nanoribbon¹⁷ and the nanodisk¹⁸ to search for zero-energy states. Then, we point out that phosphorene is a second-order HOTI, although it has so far been

regarded as a trivial insulator due to the absence of topological boundary states. This may well be the first example of HOTIs whose samples are already available in laboratories. It is also possible to construct a 3D crystal (anisotropic diamond lattice) so that its boundary is the above 2D crystal (anisotropic honeycomb lattice) when we cut it along a plane. Then, it is a third-order TI by definition. These anisotropic lattice models are higher-dimensional extensions of the SSH model.

Minimal two-band models

HOTIs were originally proposed on square lattices with the use of the four-band model³⁻¹¹, and subsequently studied on the breathing Kagome and pyrochlore lattices with the use of the three-band and four-band models¹², respectively. The minimal model to describe insulators is the two-band model. We propose a two-band model to reveal the essence of HOTIs.

We consider lattice models which have two atoms in the unit cell. By requiring the chiral symmetry, the Hamiltonian is described by the two band theory

$$H_0 = \begin{pmatrix} 0 & F \\ F^* & 0 \end{pmatrix}, \quad (1)$$

where the chiral symmetry operator is $C = \sigma_z$ with $C^{-1}H_0C = -H_0$. The diagonal terms are prohibited by the chiral symmetry. The energy spectrum reads $E = \pm |F|$, which is symmetric ($E \leftrightarrow -E$) due to the chiral symmetry. Typical examples are the SSH model in one dimension, the anisotropic honeycomb lattice in two dimensions and the anisotropic diamond lattice in three dimensions. For the SSH model¹⁹, we take

$$F = t_a + t_b e^{ik}. \quad (2)$$

For the anisotropic honeycomb lattice, we take²⁰⁻²⁴

$$F = 2t_a e^{-ik_y/2} \cos \frac{\sqrt{3}k_x}{2} + t_b e^{ik_y}. \quad (3)$$

For the anisotropic diamond lattice, we take²⁵

$$F = t_a (e^{ik \cdot \mathbf{X}_2} + e^{ik \cdot \mathbf{X}_3} + e^{ik \cdot \mathbf{X}_4}) + t_b e^{ik \cdot \mathbf{X}_1}, \quad (4)$$

with the four lattice vectors pointing the tetrahedron directions $\mathbf{X}_1 = (1, 1, 1)$, $\mathbf{X}_2 = (1, -1, -1)$, $\mathbf{X}_3 = (-1, 1, -1)$ and $\mathbf{X}_4 = (-1, -1, 1)$. We take $t_b > 0$ without loss of generality.

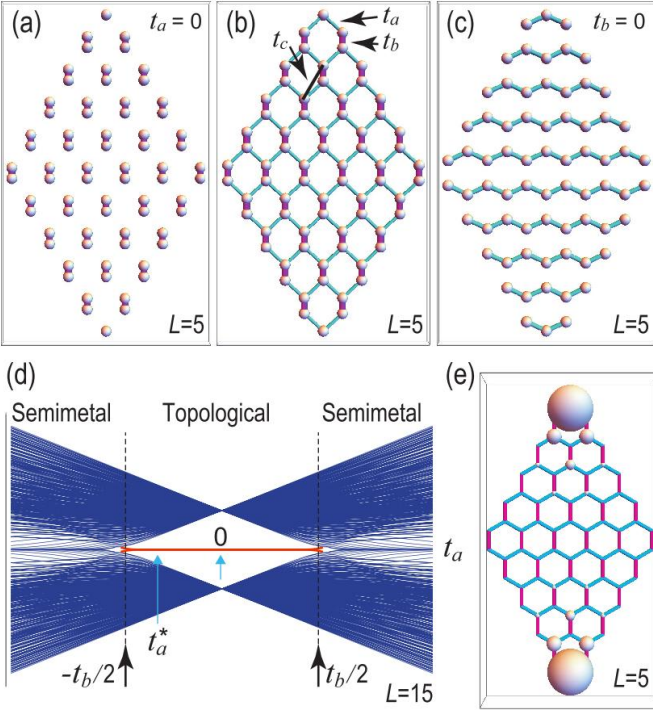


FIG. 1: Illustration of diamonds with (a) $t_a = 0$, (b) $|t_a| < t_b$ and (c) $t_b = 0$. The size L is defined by the number of Benzene rings on one side in (b). (a) There are two isolated atoms at the top and bottom corners of the diamond for $t_a = 0$. (b) All four edges form skew-zigzag nanoribbons well described by the SSH model. The two corners at the top and the bottom are topological zero-energy states inherent to the SSH model. (d) Energy spectrum of the diamond made of the anisotropic honeycomb lattice. The horizontal axis is t_a with a fixed value of $t_b = 3.665\text{eV}$, where $t_a^* = -1.220\text{eV}$. There emerge zero-energy states (marked in red) for $|t_a| < t_b/2$. They represent topological boundary states. (e) The square root of the local density of states $\sqrt{\rho_i}$ for the diamond. The amplitude is represented by the radius of the spheres. The local density of states becomes arbitrarily small except for the two corners for $L \gg 1$, indicating that the localized states emerge only at the two corners of the diamond.

In the case of the SSH model, the WC is given by the polarization p_x along the x axis, which is the bulk topological index protected by the mirror symmetry along the x direction. We generalize it to higher dimensions^{4,8,9,12}. The WC is given by the set of the j polarization p_α in the j dimensions, which is the average of the position in the unit cell,

$$p_\alpha = -\frac{1}{V} \int_{\text{BZ}} d^j k A_\alpha, \quad (5)$$

where $A_\alpha = -i \langle \psi | \partial_{k_\alpha} | \psi \rangle$ is the Berry connection, V is the volume of the Brillouin zone, and the integration is carried out over the Brillouin zone. Due to the gauge invariance of the polarization⁴, p_α is defined mod 1. Furthermore, in the presence of the mirror symmetry, $M_\alpha^{-1} H_0(k_\alpha) M_\alpha = H_0(-k_\alpha)$, the polarization is odd⁴, $p_\alpha \rightarrow -p_\alpha$, with respect to it. Combining these two properties, we find^{4,8,9,12} that the polarization p_α is quantized to be 0 or $1/2$.

The topological nature of the polarization is made man-

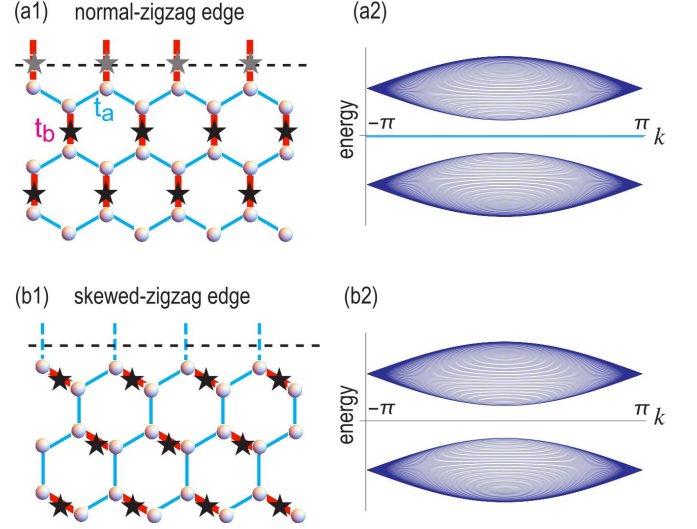


FIG. 2: Illustration and band structure of (a1,a2) a normal-zigzag nanoribbon and (b1,b2) a skewed-zigzag nanoribbon with $t_a = -1.220\text{eV}$ and $t_b = 3.665\text{eV}$. Star symbols represent WCs in (a1,b1). The horizontal axis is k in (a2,b2). (a2) When the edge cuts through WCs as in (a1), a perfect flat band emerges at zero energy as represented by a cyan line. This perfect flat band is detached entirely from the bulk band, and it does not represent a topological boundary state. (b2) When the edge cuts through no WCs as in (b1), no boundary states emerge at zero energy.

ifest for the chiral symmetric two-band theory. Using the Hamiltonian (1) explicitly, we may solve for the eigen function of the ground state as $\psi = (-e^{-i\Theta}, 1)^t / \sqrt{2}$ with $\Theta = i \log(F/|F|)$. The connection reads $A_\alpha = -\frac{1}{2} \partial_{k_\alpha} \Theta$, and hence the formula (5) represents the winding number.

We use the WC as the bulk topological number. We consider the atomic insulator limit¹³⁻¹⁶ by taking $t_a = t_b = 0$, where there are no interactions among any lattice sites, and we find $p_\alpha = 0$ trivially. Hence, when $p_\alpha = 0$ for all α , it is natural to define that the system is trivial, and otherwise topological¹³⁻¹⁶. As we shall show, the WC is $1/2$ for the SSH model, $(0, 1/2)$ for the anisotropic honeycomb lattice and $(1/2, 1/2, 1/2)$ for the anisotropic diamond lattice. They exist at the center of the dimerized bonds. The WC cannot change its value as long as the bulk band gap does not close as a function of t_α/t_b .

Phosphorene

The anisotropic honeycomb lattice is naturally realized in phosphorene²⁴, which is a monolayer material of black phosphorus. In phosphorene, there is an additional term f to the anisotropic honeycomb lattice model (1),

$$H = H_0 + fI, \quad (6)$$

where I is the 2×2 identity matrix and

$$f = 4t_c \cos \frac{\sqrt{3}}{2} k_x \cos \frac{1}{2} k_y. \quad (7)$$

Three hopping parameters t_a , t_b and t_c are shown in Fig.1, which are $t_a = -1.220\text{eV}$, $t_b = 3.665\text{eV}$, $t_c = -0.105\text{eV}$

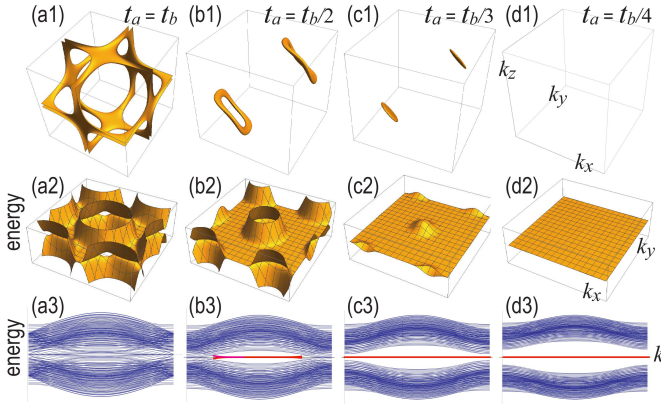


FIG. 3: The Fermi surface of the bulk anisotropic diamond lattice with (a1) $t_a = t_b$, (b1) $t_a = t_b/2$, (c1) $t_a = t_b/3$ and (d1) $t_a = t_b/4$. (a2)-(d2) The corresponding band structure of a thin film. (a3)-(d3) The corresponding band structure of a diamond prism. The size of the diamond is $L = 3$.

according to Ref.²⁶. We have checked numerically that the neglected terms do not affect the topological argument at all.

The diagonal term fI breaks the chiral symmetry and modifies the perfect flat band [Fig.2(a2)] into the quasi-flat band characteristic to phosphorene²⁴. This anisotropic two-band model may well capture the essential physics of phosphorene near the Fermi level, where $t_a/t_b \approx -1/3$. Since the diagonal term fI only shifts the energy levels by f without affecting the topological structure, it is enough to analyze the Hamiltonian H_0 to reveal the topological aspect of phosphorene.

We now show that the two-band model H_0 describes a second-order TI in the range of parameters $|t_a| < t_b/2$ by making four-step arguments. We calculate the energy spectra for the bulk, the nanoribbon and the nanodisk in the first three steps. Finally we make the topological arguments.

(i) First, we examine the bulk band spectrum. The dispersion relation reads

$$E = \pm \sqrt{t_b^2 + 4 \left(t_a^2 + t_a t_b \cos \frac{\sqrt{3}}{2} k_x \right) \cos \frac{k_y}{2}}, \quad (8)$$

Two Dirac cones exist at the K and K' points $(0, \pm k_D)$ with

$$k_D = 2 \arctan \left(\sqrt{4t_a^2 - t_b^2/t_b} \right) \quad (9)$$

for $|t_a| > t_b/2$ and the system is semimetallic. The two Dirac cones merge at the Γ point for $|t_a| = t_b/2$, and the system becomes an insulator for $|t_a| < t_b/2$.

ii) Second, we study the energy spectrum of the 1D boundary. Let us cut a crystal along a line to create a normal-zigzag edge, where the edge passes through the WCs, as in Fig.2(a1). Actually we analyze the band structure of a normal-zigzag nanoribbon²⁴. There exists a partial flat band connecting the K and K' points for $|t_a| > t_b/2$. It becomes a perfect-flat zero-energy edge state for $|t_a| < t_b/2$: See Fig.2(a2). However, they are not topological edge states implied by the conventional bulk-edge correspondence, since they are entirely

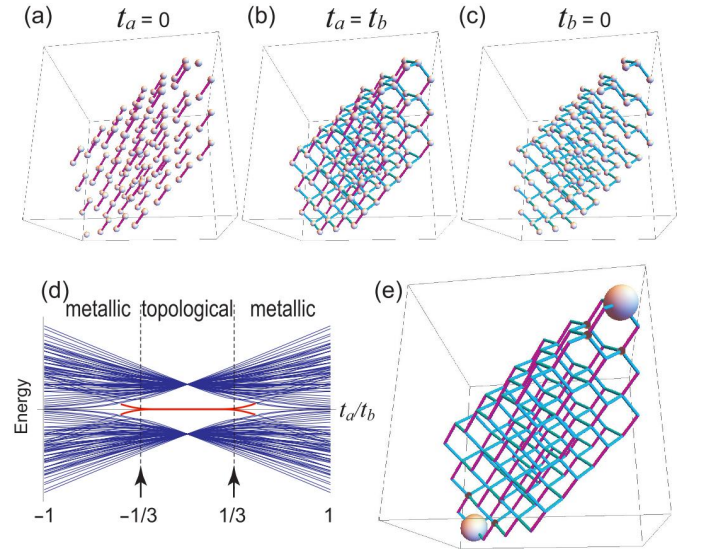


FIG. 4: Illustration of a rhombohedron made of the diamond lattice with (a) $t_a = 0$, (b) $t_a = t_b$ and (c) $t_b = 0$. (d) Energy spectrum of the rhombohedron made of the anisotropic diamond lattice with $L = 3$. The horizontal axis is t_a/t_b . There emerge zero-energy states (marked in red) for $|t_a/t_b| < 1/3$. They are topological boundary states. (e) The square root of the local density of states $\sqrt{\rho_i}$ for the rhombohedron with $L = 3$ and $t_a/t_b = 1/4$. The amplitude is represented by the radius of the spheres. The local density of states becomes arbitrarily small except for the two corners for $L \gg 1$. The localized states emerge only at the two corners of the rhombohedron.

detached from the bulk band. The emergence of the zero-energy edge states is understood as follows. The WC exists at the middle of the bond connecting the A and B sites in the topological phase: See Fig.2(a). The charge distributes in the vicinity of the WC. A half charge emerges at the boundary since the charge is separated into two pieces by the boundary on the WCs, yielding zero-energy boundary states protected by the chiral symmetry.

We may also study the energy spectrum of a skew-zigzag nanoribbon²⁷: See Fig.2(b1). A crucial difference is the absence of a zero-energy edge state: See Fig.2(b2). One edge of a nanoribbon realizes a SSH chain. The absence of the zero-energy edge states is understood as follows. The edge passes through no WCs when we cut a crystal along a line to create a skew-zigzag edge, as in Fig.2(b1). No charge emerges at the edge since there are no charge at the boundary away from the WCs.

iii) Third, we study the energy spectrum of the 0D boundary. In contrast to the 1D boundary, the zero-energy boundary states emerge at the corners of a nanodisk respecting the mirror symmetries, which are topological as in the case of the SSH model¹⁹. We cut a crystal along two lines to create two edges and one corner. These edges are skew-zigzag type to respect the two mirror symmetries. Actually we analyze the band structure of a nanodisk respecting the mirror symmetries, which is a 0D crystal. The simplest one is the diamond structure with four skew-zigzag edges as in Fig.1(d). Corner zero-energy states emerge at the top and bottom lattice sites for

$|t_a| < t_b/2$, as in Fig.1(e). When we put one electron into the zero-energy states, the $1/2$ fractional charge appears at each of the two corners of the diamond. They are absorbed in metallic phase for $|t_a| > t_b/2$. These corner zero-energy states are topological as in the case of the SSH model¹⁹, breathing Kagome and breathing Pyrochlore lattices²⁴. Namely, we find that SSH chains are realized at the four edges of the diamond structure. Consequently, the system is a second-order TI.

(iv) Finally, we study the bulk topological index characterizing the HOTI. We first investigate the extreme case of $t_a = 0$. The eigen function for the valence band is given by $\psi = (-e^{ik_y}, 1)/\sqrt{2}$. The Berry connections are obtained as $A_x = 0$ and $A_y = 1/2$, which yields the polarization $p_x = 0$ and $p_y = 1/2$. Since the position of the WC is fixed within one topological phase, we obtain the same result for $|t_a| < t_b/2$. The gap closes at $|t_a| = t_b/2$, and the system becomes semimetallic for $|t_a| > t_b/2$ as shown in Fig.1(d).

Anisotropic diamond lattice

We proceed to investigate the anisotropic diamond lattice in three dimensions. We make the five-step arguments.

i) The bulk band spectrum reads

$$\begin{aligned} E^2 = & t_a^2 + 3t_b^2 + 2t_b^2 \cos 2(k_x - k_y) + 2t_b^2 \cos 2(k_y - k_z) \\ & + 2t_b^2 \cos 2(k_z - k_x) + 2t_a t_b \cos 2(k_x + k_y) \\ & + 2t_a t_b \cos 2(k_y + k_z) + 2t_a t_b \cos 2(k_z + k_x). \end{aligned} \quad (10)$$

We show the Fermi surface in Fig.3(a1)-(d1). The Fermi surface becomes a loop node for $t_b/3 < |t_a| < t_b$, whose radius shrinks as the ration $|t_a/t_b|$ decreases as in Fig.3(b1) and (c1). The system becomes an insulator for $|t_a| < t_b/3$ as in Fig.3(d1).

ii) We calculate the surface band structure of a thin film in the $[111]$ direction corresponding to the $(j-1)$ D geometry with $j = 3$. Zero-energy partial flat bands appear whose boundary is the projection of the loop node onto the $[111]$ direction for $t_b/3 < |t_a| < t_b$: See Fig.3(b2) and (c2). It becomes a perfect flat band for $|t_a| < t_b/3$ corresponding to the

fact that the the system becomes an insulator: See Fig.3(d2).

iii) We next calculate the band structure of a diamond prism corresponding to the $(j-2)$ D geometry with $j = 3$. As in the case of the thin film, we find zero-energy partial flat bands for $t_b/3 < |t_a| < t_b$ [Fig.3(b3), (c3)], and zero-energy perfect flat bands for $|t_a| < t_b/3$ [Fig.3(d3)].

iv) We investigate the energy spectrum of the rhombohedron made of the diamond lattice, which corresponds to the $(j-3)$ D geometry with $j = 3$: See Fig.4. The energy spectrum as a function of t_a/t_b is shown in Fig.4(d). The zero-energy states emerge for $|t_a| < t_b/3$. The emergence of the zero-energy states are naturally understood by considering the extreme case with $t_a = 0$. In this case the two atoms at the top and bottom of the rhombohedron are perfectly isolated as shown in Fig.4(a). The $1/2$ fractional charge appears at each of the two corners of the rhombohedron as shown in Fig.4(e). These zero-energy states are protected by the chiral symmetry and remain as they are as long as the bulk band gap does not close.

v) We finally analyze the WC. It is easy to derive this at $t_a = 0$, where the eigen function for the valence band is given by $\psi = (-e^{i(k_x+k_y+k_z)}, 1)/\sqrt{2}$. The WC is calculated as $(1/2, 1/2, 1/2)$ for $|t_a| < t_b/3$. The gap closes at $|t_a| = t_b/3$, and the system becomes semimetallic for $|t_a| > t_b/3$, as shown in 4(d).

Discussions

We have proposed minimal HOTI models. We have argued that phosphorene is a second-order topological insulator. The construction of a HOTI based on a nontrivial WC will be applicable to other lattices with dimerizations.

Acknowledgement

The author is very much grateful to N. Nagaosa for helpful discussions on the subject. This work is supported by the Grants-in-Aid for Scientific Research from MEXT KAKENHI (Grant Nos.JP17K05490 and JP15H05854). This work is also supported by CREST, JST (JPMJCR16F1).

- ¹ M. Z. Hasan and C. L. Kane, Rev. Mod. Phys. **82**, 3045 (2010).
- ² X.-L. Qi and S.-C. Zhang, Rev. Mod. Phys. **83**, 1057 (2011).
- ³ F. Zhang, C.L. Kane and E.J. Mele, Phys. Rev. Lett. **110**, 046404 (2013).
- ⁴ W. A. Benalcazar, B. A. Bernevig, and T. L. Hughes, 10.1126/science.aah6442.
- ⁵ F. Schindler, A. Cook, M. G. Vergniory, and T. Neupert, in APS March Meeting (2017).
- ⁶ Y. Peng, Y. Bao, and F. von Oppen, Phys. Rev. B **95**, 235143 (2017).
- ⁷ J. Langbehn, Y. Peng, L. Trifunovic, F. von Oppen, and P. W. Brouwer, Phys. Rev. Lett. **119**, 246401 (2017).
- ⁸ Z. Song, Z. Fang, and C. Fang, Phys. Rev. Lett. **119**, 246402 (2017).
- ⁹ W. A. Benalcazar, B. A. Bernevig, and T. L. Hughes, Phys. Rev. B **96**, 245115 (2017).
- ¹⁰ F. Schindler, A. M. Cook, M. G. Vergniory, Z. Wang,

- S. S. P. Parkin, B. A. Bernevig, and T. Neupert, cond-mat/arXiv:1708.03636 (2017).
- ¹¹ M. Lin and T. L. Hughes, arXiv:1708.08457.
- ¹² M. Ezawa, cond-mat/arXiv:1709.08425, Phys. Rev. Lett. (to be published).
- ¹³ H. C. Po, H. Watanabe and A. Vishwanath, arXiv:1709.06551.
- ¹⁴ H. C. Po, H. Watanabe, M. P. Zaletel, and A. Vishwanath, Sci. Adv. **2** (2016).
- ¹⁵ H. C. Po, A. Vishwanath, and H. Watanabe, Nature Communications **8**, 50 (2017).
- ¹⁶ B. Bradlyn, L. Elcoro, J. Cano, M. G. Vergniory, Z. Wang, C. Felser, M. I. Aroyo, and B. A. Bernevig, Nature **547**, 298 (2017).
- ¹⁷ M. Ezawa, Phys. Rev. B, **73**, 045432 (2006).
- ¹⁸ M. Ezawa, Phys. Rev. B **76**, 245415 (2007).
- ¹⁹ W. P. Su, J. R. Schrieffer, and A. J. Heeger, Phys. Rev. Lett. **42**, 1698 (1979).
- ²⁰ B. Wunsch, F. Guinea and F. Sols, New J. of Phys., **10**, 103027

- (2008).
- ²¹ G. Montambaux, F. Piechon, J.-N. Fuchs, and M. O. Goerbig, Phys. Rev. B **80**, 153412 (2009).
- ²² V.M. Pereira, A.H. Castro Neto and N.M.R. Peres, Phys. Rev. B **80**, 045401 (2009).
- ²³ G. Montambaux F. Piéchon, J.-N. Fuchs, and M. O. Goerbig, Phys. Rev. B **80**, 153412 (2009).
- ²⁴ M. Ezawa, New J. Phys. **16**, 115004 (2014).
- ²⁵ R. Takahashi and S. Murakami, Phys. Rev. B **88**, 235303 (2013).
- ²⁶ N. Rudenko and M.I. Katsnelson, Phys. Rev. B **89**, 201408 (2014).
- ²⁷ M. M. Grujic, M. Ezawa, M. Z. Tadic, F. M. Peeters, Phys. Rev. B **93**, 245413 (2016).